Available online at www.sciencedirect.com

ScienceDirect

Procedia CIRP 112 (2022) 352–357

www.elsevier.com/locate/procedia

14th CIRP Conference on Intelligent Computation in Manufacturing Engineering, Gulf of Naples, Italy

On the Lack of fusion porosity in L-PBF processes

Stefania Cacace[a]*, Quirico Semeraro[a]

Dipartimento di Meccanica, Politecnico di Milano, Via La Masa 1 20156 Milano (Italy)

* Corresponding author. Tel.: 39 02 2399 8533; *E-mail address:* stefania.cacace@polimi.it

Abstract

Lack of fusion porosity is a typical defect of laser powder bed fusion processes generated by a wrong selection of process parameters that do not ensure a proper overlapping of melt pools. Melt pool dimensions and lack of fusion porosity can be predicted using analytical models that use as inputs material properties and process parameters. None of these models considers the variability of the melt pool dimensions in predicting the lack of fusion porosity. In this work, Monte Carlo simulations are used to determine the influence of the variability of the melts pools dimensions on the selection of process parameters.

Peer-review under responsibility of the scientific committee of the 15th CIRP Conference on Intelligent Computation in Manufacturing Engineering, 14-16 July, Gulf of Naples, Italy

Keywords: Selective Laser Melting; Lack of fusion; Process parameters

Nomenclature

BR	Build Rate (cm^3/h)
D	Melt pool depth (mm)
E_d	Energy density (J/mm^3)
H	Hatch distance (mm)
L	Layer thickness (mm)
P	Laser Power (W)
a	Beam radius (mm)
d_p	Point distance (mm)
h_s	Enthalpy at melting (J/m^3)
t	Exposure time (μs)
u	Laser Speed (m/s)
α	Thermal diffusivity (m^2/s)

1. Introduction

Laser-based Powder Bed Fusion processes (L-PBF) emerged as a leading technology to produce critical components in the automotive and aerospace industry [1]. This technology allows the production of metal parts with a high degree of geometric complexity, ensuring cost reduction [2]. However, L-PBF processes still lack a large implementation in industrial practice, mainly due to the high initial costs for equipment and powder and the limited portfolio of materials available.

Due to the complexity of the L-PBF processes, the selection of process parameters is carried out for each specific material. The interaction between the powder particles and the laser determines the properties of the final part. Depending on the material properties (absorptivity, thermal conductivity, heat capacity), the combination of process parameters ensure the complete melting of the powder changes [3].

The process parameters usually involved in the optimization are power P, laser speed u, hatch distance H, and layer thickness L. These are combined to determine the Energy density, which determines the amount of Energy delivered from the laser to the powder bed [4]. The Energy density (J/mm^3) is defined as:

$$E_d = \frac{P}{u \cdot H \cdot L} \tag{1}$$

Energy density predicts the apparent density of the printed parts, as shown in Figure 1 [5]. It is now well-known that a low value of Energy density leads to the formation of a lack of fusion porosity due to the incomplete melting of the powder. Excessive Energy leads to the formation of keyhole porosity. Energy density is also closely related to the productivity of the

Peer-review under responsibility of the scientific committee of the 15th CIRP Conference on Intelligent Computation in Manufacturing Engineering, 14-16 July, Gulf of Naples, Italy
10.1016/j.procir.2022.09.008

process: the build rate (BR) is proportional to P/E_d. Energy density should be reduced to increase productivity, but there is a lower limit for this reduction that is the limit for lack of fusion formation, E_{min}. The feasibility window for the L-PBF process is identified by the range of Energy density where apparent density is constant at around 99% of the reference material.

The selection of the optimal process parameters can be determined using an experimental approach, numerical modeling, or analytical models. Experiments and numerical modeling are computational and time expensive. The experimental approach allows to study the variability of the process and multiple outputs simultaneously: density, porosity, microstructure, residual stresses, for example.

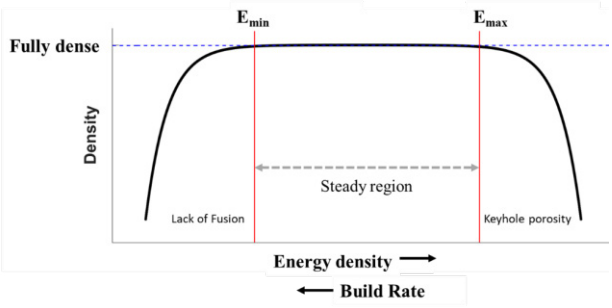

Fig. 1. Variation of apparent density with Energy density in L-PBF processes.

The need to increase the material available for this technology calls for implementing a faster procedure to determine a feasibility window that at least ensures high-density parts. Analytical models can be effectively applied to determine the process window for material that was not previously tested with L-PBF technologies only based on the material physical properties.

However, these models do not consider the variability that affects all manufacturing processes, which is a crucial problem as the reproducibility of the L-PBF processes has been questioned [6]. Powder layering, absorptivity, spatter all influence the stability of the process and, therefore, the final part properties [7]. The thermal analytical models usually used in L-PBF processes are deterministic. For a set of process parameters and material properties, the output is of the size of the melt pool, namely depth D and width W [8]. Literature data show that the melt pool size changes even when using constant process parameters due to powder layering, particle properties, and spatter. These phenomena also influence 3D printed parts, as even at optimal process parameters, defects can still be present [9]. For this reason, it is essential to include in analytical models the inevitable variability of the process to determine the feasible processing window.

In this work, analytical models are used to predict the melt pool dimensions, and a Monte Carlo approach is used to simulate the melt pool size variability. Simulated melt pool geometries are then used to evaluate the probability of forming the lack of fusion porosity based on the geometrical model proposed by [10]. The objective is to identify a processing window that allows to minimize the probability of defect formation and maximize productivity. Analytical models are validated using experimental results.

The paper is organized as follows: In Section 2.1, the analytical model for the melt pool and the geometrical model for lack of fusion porosity are discussed. In Section 2.2, the Monte Carlo approach is presented along with the method for the calculation of the probability of lack of fusion. In Section 2.3, the experimental design is discussed in Section 3. The results of the simulation are presented, along with the comparison with the experimental data. Eventually, the feasibility region is derived.

The schematization of the work is illustrated in Figure 2.

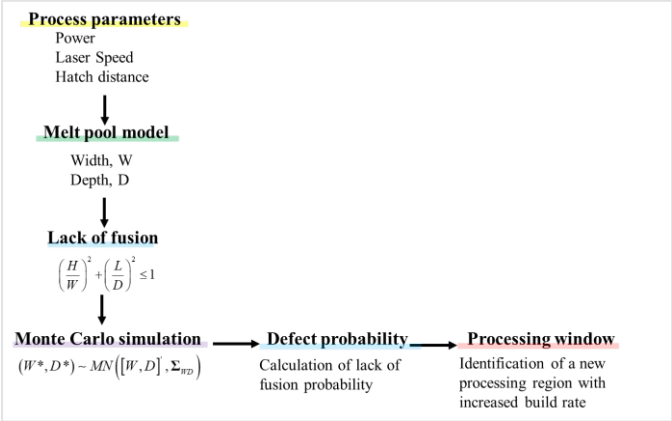

Fig. 2. Schematization of the workflow

2. Analytical models for melt pool and defect generation

2.1. Analytical model for melt pool dimension and defect formation

The melt pool dimension depends on the process parameters of the L-PBF process (power and scan speed) and the material properties (conductivity and diffusivity). For the present work, the melt pool dimensions were estimated using the Rosenthal equation [11]. The Rosenthal equation is based on several assumptions that do not influence its ability to accurately predict the melt pool geometry [10]. A complete discussion of the Rosenthal equation can be found in [8]. The calculations performed in this work are based on the formulation provided by [8] and [12]. Gaussian distribution of the heat source was considered, and normalized terms were introduced to simplify the analysis. The final analytical form used to predict the melt pool dimensions is shown in Eq (2).

$$g=\int_0^{\infty}\frac{\exp\left[-\frac{z'^2}{4t}-\frac{y'^2+(x'-t)^2}{4pt+1}\right]}{(4pt+1)\sqrt{t}}dt \qquad (2)$$

Where g is the function that described the temperature distribution in function of spatial coordinates (x, y, z) and parameter p. Spatial coordinates are normalized as x'=x/a, y'=y/a, and $z'=z(\alpha/ua)^{-0.5}$, where u is the laser speed, a is the laser radius and D is the thermal diffusivity. The variable t is normalized with (a/u). Parameter p is defined as D/(ua).

The Eq (2) result is the geometry of the melt pool dimensions, namely melt pool depth, D, and melt pool width, W. There is one combination of melt pool size in output for a given set of input data of laser and material parameters.

D and W are used in the defect model proposed by Tang et al. [10]. to predict the lack of fusion porosity. The melt pool is

approximated by a dual half-elliptical cross-sectional shape, as shown in Figure 3. The basic idea behind this model is that the condition for avoiding the lack of fusion porosity is that the melt pool width is larger than the hatch space and that the melt pool depth is larger than the layer thickness. These two conditions ensure no formation of porosity between adjacent melt pools and that there is re-melting of the previous layer. The condition used for lack of fusion formation is:

$$\left(\frac{H}{W}\right)^2+\left(\frac{L}{D}\right)^2\le 1 \qquad (3)$$

Where H is the hatch distance, L is the layer thickness, W is the melt pool width and D is the melt pool depth. If the combination of the process parameters (H, L) and the melt pool dimension (W, D) does not meet the condition in Eq (3), lack of fusion porosity is formed in the final part, which eventually indicates that the Energy density used is lower than E_{min}.

King et al. [12] showed that Eq (2) can be rewritten also in the form of normalized enthalpy as follows:

$$\frac{\Delta H}{h_s}=\frac{AP}{h_s\sqrt{\pi\alpha u a^3}} \qquad (4)$$

Normalized enthalpy can be used to determine the presence of keyhole porosity, that is defining the maximum level of Energy density (E_{max}) that belongs to the steady region, visible in Figure 1.

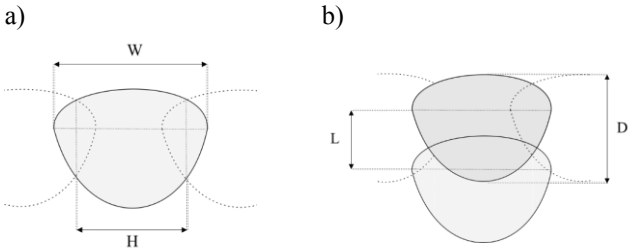

Fig. 3. Schematic visualization of the melt pool geometry a) hatch distance and melt pool width; (b) layer thickness and melt pool depth.

2.2. Simulation and lack of fusion porosity

A Monte Carlo approach is used to incorporate variability in the definition of the condition for lack of fusion formation. Melt pool depth and width are correlated, so for the simulation a Multi-Normal distribution is considered. The mean vector of the distribution is the output of the analytical model in Eq (2) $\boldsymbol{\mu} = [W, D]^T$ and the variance-covariance matrix $\boldsymbol{\Sigma}_{WD}$ was estimated based on literature data [13]. The estimated value of $\boldsymbol{\Sigma}_{WD}$ is equal to

$$\Sigma_{WD}=\begin{bmatrix} 3.3887 & -4.4314 \\ -4.4314 & 6.6100 \end{bmatrix}$$

In conclusion, melt pool dimensions are generated according to the following statistical model:

$$\left[W^*, D^*\right] \sim MN\left(\left[W, D\right]', \boldsymbol{\Sigma}_{\mathbf{WD}}\right)$$

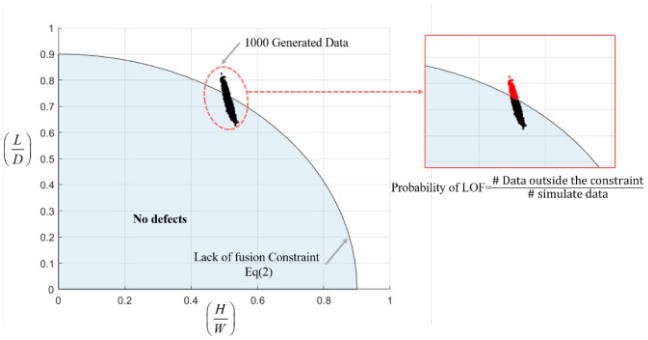

Fig. 4. Probability of lack of fusion.

All the simulated melt pools do not necessarily meet the condition in Eq (3). Consequently, the result of the simulation indicates a probability of lack of fusion formation. This probability is calculated as the percentage of melt pool sizes that do not meet the condition in Eq (3). The generated data (H/W*) and (L/D*) are shown as black dots in Figure 4; in the magnification on the right, data that do not satisfy the constraint in Eq (3) are plotted in red. The probability of lack of fusion is estimated as the number of red points over the total number of simulated data.

For the present work, 1000 melt pool sizes [W*, D*] were generated. A sensitivity analysis was carried out to define the number of data to generate. The error in determining the lack of fusion probability varied less than 0.5% when the number of generated data was increased to 10000. One thousand generated data were therefore used to reduce the computational time.

2.3. Experimental Validation

The lack of fusion limit Eq (3) and keyhole boundary in Eq (4) are compared to experimental data to validate the current approach. AISI 316L specimens were produced using an industrial L-PBF system, Renishaw AM 250. Process parameters were varied at four levels of Energy density, 34, 59 103 to 180 J/mm3. Different combinations of process parameters (power, scan speed, and hatch distance) were used for each combination of Energy density. The layer thickness was kept constant at 0.05 mm. Renishaw AM250 is equipped with a pulsed laser, so the laser speed is a function of two other parameters: point distance d_p and exposure time t. The following relationship was used to convert point distance and exposure time into laser speed:

$$u=\frac{d_p}{\frac{dp}{JS}+t} \qquad (5)$$

JS is the jump speed, that is the speed at which the laser moves from one spot to the other along the same scan line (Figure 5); JS was set at 4000 mm/s.

The beam diameter is approximately 70 µm, so the beam radius considered for the calculations is a=35 µm.

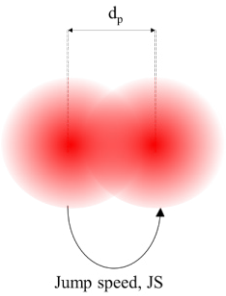

Fig. 5. Conversion from point distance, hatch distance and jump speed to laser speed.

Apparent density was measured using Archimedes method, considering three replicated for each measurement.

The input parameters used for the analytical model in Eq (1) are shown in Table 1.

Table 1. AISI 316L material properties used for the evaluation of Eq (2).

Property	Value	MU
Heat Capacity	460	J/Kg/K
Density	7980	Kg/m^3
Melting temperature	1673	K
Absorption	0.35	-
Thermal diffusivity	5.38 e-06	m^2/s
Enthalpy at melting	9.8	KJ/cm^3

3. Results

3.1. Validation of the analytical model

The apparent density results for the validation of the analytical models are shown in Figure 6.

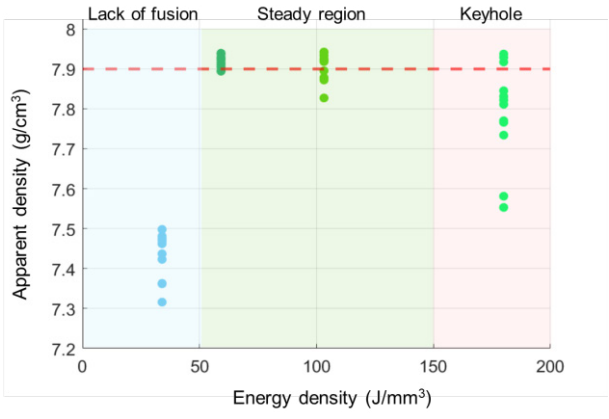

Fig. 6 AISI 316L apparent and relative density result. A horizontal dotted line defines a 99% relative density. The reference value for bulk density of the material is 7.98 g/cm^3.

The large range of Energy density considered shows clearly the minimum and maximum value of Energy density that define the steady region. Full densification is obtained between 59 and 103 J/mm^3, while keyhole porosity is responsible for the low apparent density values at 180 J/mm^3.

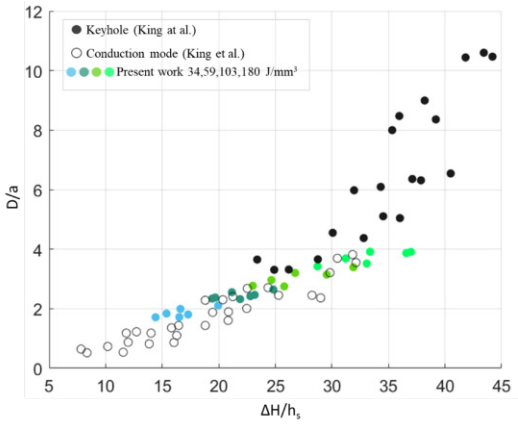

Fig. 7 Melt pool depth normalized by beam size (D/a) as function of the normalized enthalpy ($\Delta H/h_s$). Comparison between the literature data [12] and experimental data.

Lack of fusion phenomena is present at the lowest value of Energy density.

The data provided by King et al. in [12] were used to validate the results obtained from Eq (4) for AISI 316L. The results are shown in Figure 7. According to [12], the keyhole threshold was obtained at $\Delta H/h_s \approx (30 \pm 4)$; our experiment confirms this threshold as the apparent density of samples produced at 180 J/mm^3 results in a normalized enthalpy range between 25 and 35.

The Eq (3) model effectively predicts the lack of fusion limit (Figure 8), all samples built at the lowest value of Energy density lie outside or on the limit., all samples built at the lowest value of Energy density lie outside or on the limit. Samples produced at E_d=34 J/mm^3 are clearly in the lack of fusion region; however, they are still on the boundary defined by Eq (3). This result might be due to the lack of precision of some input parameters in Table 1, such as absorptivity or the conversion used for the speed in Eq (5) that inevitably produce errors in Eq's analytical solution (2). However, the correspondence between the analytical models and the experimental results is quite good.

The validation of the analytical model using experimental results is completed. Both Eq (3) and Eq (4) effectively determine the limits for the stability region of Energy density. In the next Section, the results of the Monte Carlo simulation are illustrated.

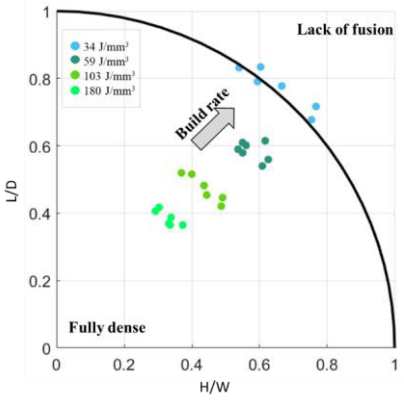

Fig 8. identification of the lack of fusion limit using Eq (3).

3.2. Monte Carlo simulation results

By moving towards the lack of fusion limit in Fig. 8, the Build Rate increases. Therefore, the selection of the process parameters window implies the maximization of the BR, limited by the possible formation of lack of fusion porosity. Monte Carlo simulation is used to identify if it is possible to increase the BR of the process by minimizing the probability of formation of lack of fusion using the procedure described in Section 2.2. Based on the experimental results, it is possible that an anergy density between 34 J/mm^3 and 53 J/mm^3 could ensure the maximization of the BR with a minimum probability of lack of fusion.

The simulation involves calculating the lack of fusion probability for selected combinations of parameters in the Energy density range between 34 and 53 J/mm^3. The Energy density value selected was 34, 38, 46, and 50 J/mm^3. Ten combinations of process parameters (P, u, H) were generated for each value of Energy density, five using P=150 W and five using P = 200 W. So, a total number of 50 simulations was carried out. A large variation of process parameters was selected for the simulation. (0.2≤u≤0.9 mm/s and 0.075≤H ≤ 0.124 mm). The layer thickness was kept constant at 0.05 mm.

The results of the simulation are shown in Fig.9 and Table 2.

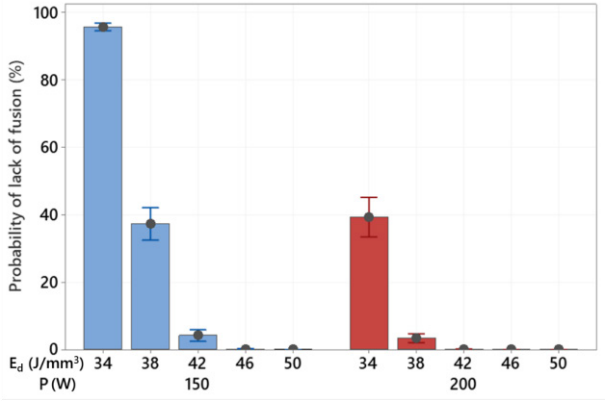

Fig.9 Lack of fusion probability resulting from Monte Carlo simulation at different values of Energy density and power.

The results of the simulation show that at higher Power level the limit for fully densification is obtained at a lower Energy density level. The probability of lack of fusion at E_d = 42 J/mm^3 for P = 200 W is 0.1 % compared to 4.2 % for P=150 W.

This result differs from previous works ([4] [14]) that suggest that Energy density is a valid descriptor of the densification mechanism in L-PBF processes independently from the combination of process because of the large variation of process parameters considered in this simulation.

In conclusion, based on the simulation results it is possible to identify an enlarged Energy density stability region for AISI 316L. It is possible to select E_d=46 J/mm^3 to production fully dense samples by reducing the probability of formation of lack of fusion and increasing the build rate of the process.

4. Conclusions

. In this work, Monte Carlo simulation is used to study the influence of the variability of melt pool size on the Energy density feasibility region. Experimental data were used to validate the analytical and geometrical models that determine the minimum and maximum Energy density levels for L-PBF processes. The experimental results are coherent with the limit indicated by the literature for lack of fusion and keyhole porosity.

Melt pool dimensions were generated using a Multi-Normal distribution. The resulting probability of formation of lack of fusion for a range of Energy density between 34 and 50 J/mm3 was studied to identify a new processing region with increased productivity.

The simulation results showed that using a high value of Power allows a selection of parameters with an increased build rate. Additionally, different process parameters resulting in the same Energy density result in a similar lack of fusion probability.

Table 2. AISI 316L material properties used for the evaluation of Eq (1).

Power (W)	E_d (J/mm^3)	Lack of fusion probability (%) ±1 std
150	34	95.7 ± 2.5
	38	37.3 ± 10.8
	42	4.2 ± 3.8
	46	0.2 ± 0.2
	50	0.0 ± 0.0
200	34	39.3 ± 13.1
	38	3.4 ± 3.0
	42	0.1 ± 0.2
	46	0.0 ± 0.0
	50	0.0 ± 0.0

Acknowledgements

The Italian Ministry of Education, University and Research is acknowledged for the support provided through the Project "Department of Excellence LIS4.0 - Lightweight and Smart Structures for Industry 4.0”.

References

[1] R. Singh, A. Gupta, O. Tripathi, S. Srivastava, B. Singh, A. Awasthi, S.K. Rajput, P. Sonia, P. Singhal, K.K. Saxena, Powder bed fusion process in additive manufacturing: An overview, Mater. Today Proc. 26 (2019) 3058–3070. https://doi.org/10.1016/j.matpr.2020.02.635.

[2] R.E. Laureijs, J.B. Roca, S.P. Narra, C. Montgomery, J.L. Beuth, E.R.H. Fuchs, Metal additive manufacturing: Cost competitive beyond low volumes, J. Manuf. Sci. Eng. Trans. ASME. 139 (2017) 1–9. https://doi.org/10.1115/1.4035420.

[3] H. Ghasemi-Tabasi, J. Jhabvala, E. Boillat, T. Ivas, R. Drissi-Daoudi, R.E. Logé, An effective rule for translating optimal selective laser melting processing parameters from one material to another, Addit. Manuf. 36 (2020)

101496. https://doi.org/10.1016/j.addma.2020.101496.
[4] S. Cacace, Q. Semeraro, Improvement of SLM Build Rate of A357 alloy by optimizing Fluence, J. Manuf. Process. 66 (2021) 115–124. https://doi.org/10.1016/j.jmapro.2021.03.043.
[5] J.P. Oliveira, A.D. LaLonde, J. Ma, Processing parameters in laser powder bed fusion metal additive manufacturing, Mater. Des. 193 (2020) 1–12. https://doi.org/10.1016/j.matdes.2020.108762.
[6] L. Dowling, J. Kennedy, S. O'Shaughnessy, D. Trimble, A review of critical repeatability and reproducibility issues in powder bed fusion, Mater. Des. 186 (2020) 108346. https://doi.org/10.1016/j.matdes.2019.108346.
[7] W. Wang, J. Ning, S.Y. Liang, Prediction of lack-of-fusion porosity in laser powder-bed fusion considering boundary conditions and sensitivity to laser power absorption, Int. J. Adv. Manuf. Technol. 112 (2021) 61–70. https://doi.org/10.1007/s00170-020-06224-7.
[8] A.M. Rubenchik, W.E. King, S.S. Wu, Scaling laws for the additive manufacturing, J. Mater. Process. Technol. 257 (2018) 234–243. https://doi.org/10.1016/j.jmatprotec.2018.02.034.
[9] Z. Snow, A.R. Nassar, E.W. Reutzel, Invited Review Article: Review of the formation and impact of flaws in powder bed fusion additive manufacturing, Addit. Manuf. 36 (2020) 101457. https://doi.org/10.1016/j.addma.2020.101457.
[10] M. Tang, P.C. Pistorius, J.L. Beuth, Prediction of lack-of-fusion porosity for powder bed fusion, Addit. Manuf. 14 (2017) 39–48. https://doi.org/10.1016/j.addma.2016.12.001.
[11] D. Rosenthal, Mathematical theory of heat distributionduring welding and cutting, Weld. J. 20 (1941) 220–234.
[12] W.E. King, H.D. Barth, V.M. Castillo, G.F. Gallegos, J.W. Gibbs, D.E. Hahn, C. Kamath, A.M. Rubenchik, Observation of keyhole-mode laser melting in laser powder-bed fusion additive manufacturing, J. Mater. Process. Technol. 214 (2014) 2915–2925. https://doi.org/10.1016/j.jmatprotec.2014.06.005.
[13] V. Gunenthiram, P. Peyre, M. Schneider, M. Dal, F. Coste, I. Koutiri, R. Fabbro, Experimental analysis of spatter generation and melt-pool behavior during the powder bed laser beam melting process, J. Mater. Process. Technol. 251 (2018) 376–386. https://doi.org/10.1016/j.jmatprotec.2017.08.012.
[14] S. Cacace, Q. Semeraro, About Fluence and Process Parameters on Maraging Steel Processed by Selective Laser Melting: Do They Convey the Same Information?, Int. J. Precis. Eng. Manuf. 19 (2018) 1873–1884. https://doi.org/10.1007/s12541-018-0204-y.